sciendo

POLISH MARITIME RESEARCH 1 (113) 2022 Vol. 29; pp. 34-42
10.2478/pomr-2022-0004

STUDY ON DYNAMIC RESPONSE OF OFFSHORE WIND TURBINE STRUCTURE UNDER TYPHOON

Junlai Li[1]
Weiguo Wu[1]
Yu Wei[2]
Yu Shu[2]
Zhiqiang Lu[2]
Wenbin Lai[2]
Panpan Jia[2]
Cheng Zhao[2]
Yonghe Xie [2 *]

[1] Wuhan University of Technology, Wuhan, China
[2] ZheJiang Ocean University," Zhoushan, China

* Corresponding author: *xieyh@zjou.edu.cn (Y. Xie)*

ABSTRACT

Floating offshore wind turbines are easily affected by typhoons in the deep sea, which may cause serious damage to their structure. Therefore, it is necessary to study further the dynamic response of wind turbine structures under typhoons. This paper took the 5MW floating offshore wind turbine developed by the National Renewable Energy Laboratory (NREL) as the research object. Based on the motion theory of platforms in waves, a physical model with a scale ratio of 1:120 was established, and a hydraulic cradle was used to simulate the effect of waves on the turbines. The dynamic response characteristics of offshore wind turbines under typhoons are systematically studied. The research results clarified that the turbine structure is mainly affected by wave loads under typhoons, and its motion response reaches its maximum value under the action of extreme wave loads. The research results of this paper can provide reference value for the design of offshore wind turbine structures under typhoons.

Keywords: floating offshore wind turbine; structural dynamic response; typhoon; physical model test

INTRODUCTION

At present, the development and utilization of renewable energy has become one of the important needs of various countries for energy development. Wind energy is a very abundant form of renewable energy with the prospect of large-scale development [1, 2]. Due to factors such as noise and insufficient ground space, the development of wind energy on land is subject to certain restrictions, so offshore wind energy has gradually attracted the attention and research of academia and industry, showing a trend of development from shallow sea to deep sea [3, 4]. Floating offshore wind turbines are new equipment for the development of deep-sea wind energy, and multi-floating offshore wind turbines have been widely used due to their excellent motion performance and self-floating stability [5, 6].

Since offshore wind turbines operate in a complex flow field combining wind and waves, they need to withstand not only aerodynamic loads above the water surface, but also wave loads below it [7, 8]. Under the coupled effect of wind and waves, especially under typhoons, the offshore wind turbine structure is likely to undergo violent motion and sustain damage. Therefore, it is necessary to study further the dynamic response of wind turbine structures under typhoons [9, 10].

Aggarwal et al. used FAST software to solve the aerodynamic load of the offshore wind turbine, and imported the model into the hydrodynamic software AQWA to simulate the dynamic response of the Spar floating offshore wind turbine when

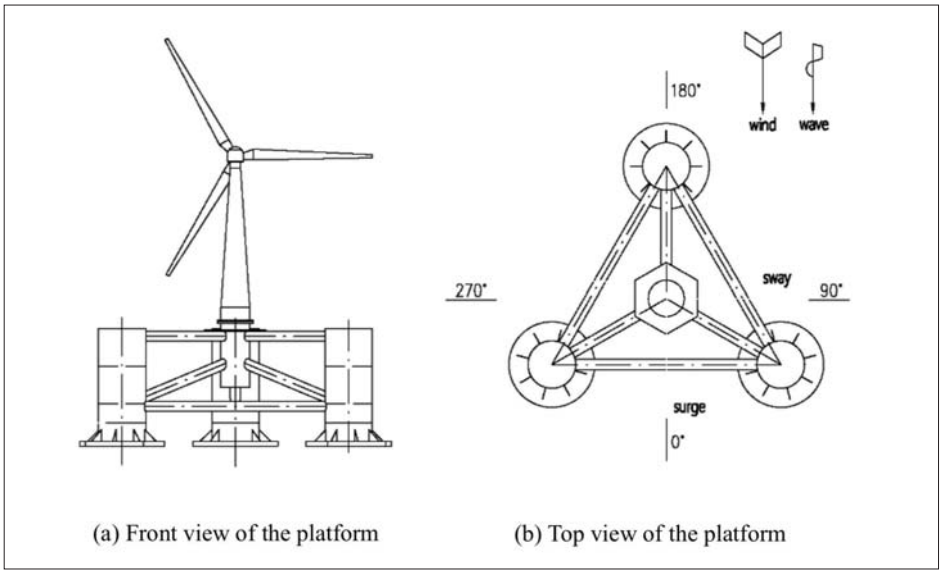

Fig. 1. Schematic diagram of the structure of NREL-5MW

subjected to wind and wave loads, but did not consider the coupled effect between the wind load and wave load [11]. Tran et al. used the CFD method to study the influence of the vortex-wake-blade coupling on the aerodynamic performance of the wind turbine, and concluded that the unsteady aerodynamic load is very sensitive to the frequency and amplitude changes of the platform motion [12]. Roddier et al. designed a three-buoy floating semi-submersible platform based on NREL-5 MW, simulated the dynamic response of the platform in the frequency domain, and analysed the applicability of the scheme [13]. Chen et al. used numerical simulation methods to study the aerodynamic characteristics of floating offshore wind turbines with different periods and wave heights, and concluded that the coupled effect of waves and wind is not conducive to the power generation of wind turbines [14]. Ishihara et al. studied the influence of wave-current coupling on the dynamic response of offshore buoyancy wind turbines, and concluded that considering the directional spreading of the sea wave spectrum can improve the prediction of the platform's dynamic response [15].

At present, there are few studies on the dynamic response of floating offshore wind turbines under typhoons, and there are insufficient physical tests. Therefore, in order to explore further the dynamic response of offshore wind turbines under typhoons, Zhejiang Ocean University established a physical model of the NREL-5MW floating offshore wind turbine with a scale ratio of 1:120. The structure of NREL-5MW is shown in the diagrams in Fig. 1.

The remainder of the paper is organised as follows: Section 2 derives the motion and force of the platform in the waves, which is the theoretical basis for the design of the hydraulic cradle. In Section 3, a physical model of the NREL-5MW floating offshore wind turbine with a scale ratio of 1:120 is established, and its structure and working principle are introduced. The reliability of the model is verified by comparing the results of the physical model test and numerical simulation. In Section 4, a series of physical model tests are carried out to systematically study the dynamic response of the offshore wind turbine structure under typhoon. Section 5 is the conclusion.

THE MOTION AND FORCE OF THE PLATFORM IN THE WAVES

BOUNDARY CONDITIONS

The potential-flow theory assumes that the fluid is ideal, there is a potential function and the fluid particles do not rotate. Enclose the wet surface S_H of the platform, free surface S_F, seabed S_B and remote control surface S_C into a space fluid domain, and record the total velocity potential as $\phi(x, y, z, t)$, which can be obtained by separating the time factor and the space factor [16, 17]:

$$\phi(x, y, z, t) = Re[\varphi e^{-i\omega t}] \tag{1}$$

where ω is the angular frequency of the incident wave, rad/s; t is time, s.

In the fluid domain φ satisfies the Laplace equation:

$$\nabla^2\varphi = 0 \tag{2}$$

Linearising the boundary conditions of the free surface, the free surface kinematics boundary equation can be written as:

$$\frac{\partial\varphi}{\partial z} - k\varphi = 0 \qquad (z = 0) \tag{3}$$

where k is the wave number, which satisfies the dispersion equation $k = \frac{\omega^2}{g}$, rad/m; g is the acceleration of gravity, 9.81 m/s^2.

The velocity potential φ of the incident wave can be expressed as:

$$\varphi = \frac{gh}{\omega} e^{kz} \sin(kz - \omega t) \tag{4}$$

where h is the water depth, m.

φ can be decomposed into the radiation part φ_R and the diffraction part φ_D:

$$\varphi = \varphi_R + \varphi_D \tag{5}$$

$$\varphi_R = i\omega \sum_{j=1}^{6} \varepsilon_j \varphi_j \tag{6}$$

$$\varphi_D = \varphi_0 + \varphi_{\exists} \tag{7}$$

where ε_j is the motion amplitude of the platform in six degrees of freedom; φ_j is the radiation potential of the corresponding unit amplitude; and the velocity potential $\varphi_{\exists}$ is the disturbance generated by the incident wave due to the stationary platform. The total diffraction potential φ_D is the sum of φ_0 and $\varphi_{\exists}$.

At the undisturbed position of the platform boundary, the diffraction potential and the radiation potential satisfy the following relationship:

$$\frac{\partial \varphi_j}{\partial n} = n_j \tag{8}$$

$$\frac{\partial \varphi_D}{\partial n} = 0 \tag{9}$$

where $(n_1, n_2, n_3) = \vec{n}$ is the unit normal vector of the wet surface S_H of the platform, and $(n_4, n_5, n_6) = \vec{r} \times \vec{n}$, $\vec{r}$ is the position vector, $\vec{r} = (x, y, z)$.

FORCE ANALYSIS OF THE PLATFORM

According to the radiation potential and diffraction potential of the three-dimensional platform, the first-order dynamic pressure acting on the platform can be written by the Bernoulli equation as:

$$p(x, y, z, t) = -\rho \frac{\partial \phi}{\partial t} = Re\left[i\rho\omega\left(\varphi_0 + \varphi_{\exists} + \sum_{j=1}^{6} \varepsilon_j \varphi_j\right) e^{-i\omega t}\right] \tag{10}$$

The force and moment of the fluid received by the platform is:

$$F_i = \iint_{S_H} p n_i ds = Re\left[\left(f_{0i} + f_{\exists i} + \sum_{j=1}^{6} T_{ij} \varepsilon_j\right) e^{-i\omega t}\right] \tag{11}$$

where f_{0i} is the force and moment of the incident wave, $f_{0i} = i\rho\omega \iint_{S_H} \varphi_0 n_i ds$, N or N.m; $f_{\exists i}$ is the force and moment of the diffracted wave, $f_{\exists i} = i\rho\omega \iint_{S_H} \varphi_{\exists} n_i ds$, N or N.m; the sum of the above two formulas is the wave excitation force and moment that the platform receives in the wave, which is called the Froude–Kriloff force and moment. T_{ij} is the radiation force and moment in the i direction that the platform receives when it is at unit speed in j motion state, $T_{ij} = i\rho\omega \iint_{S_H} \varphi_j n_i ds$, N or N.m.

The radiation force and moment can be decomposed as follows:

$$Re(T_{ij} \varepsilon_j e^{-i\omega t}) = \rho Re\left[i\rho\omega^{-i\omega t} \varepsilon_j \iint_{S_H} \varphi_j n_i ds\right] = -\ddot{X}_j u_{ij} - \dot{X}_j \lambda_{ij}$$

$$u_{ij} = \rho \iint_{S_H} Re(\varphi_j) n_i ds$$

$$\lambda_{ij} = \rho \iint_{S_H} Im(\varphi_j) n_i ds \tag{12}$$

It can be seen from the above that the radiation force and moment are composed of two parts, one of which is proportional to the acceleration of the platform, and the proportional coefficient u_{ij} is called additional mass; the other is proportional to the speed of the platform, and the proportional coefficient λ_{ij} is called the wave-making damping coefficient. $X_j (j = 1, 2, \ldots 6)$ represents the six degrees of freedom motion of the platform, which corresponds to surging, swaying, heaving, rolling, pitching and yawing respectively.

Therefore, the additional mass and wave-making damping coefficient can be used to express the force and moment of the fluid received by the platform:

$$F_i = Re\left[\left(f_{0i} + f_{\exists i}\right) e^{-i\omega t}\right] - \sum_{j=1}^{6} (\ddot{X}_j u_{ij} + \dot{X}_j \lambda_{ij}) \tag{13}$$

TIME DOMAIN MOTION EQUATION OF THE PLATFORM

According to the impulse response method proposed by Cummins, the motion of the platform at any time in the wave is regarded as superimposed by a series of instantaneous impulse motions, and the wave force at any time is regarded as the combination of a series of impulse excitations. When only the first-order wave force is considered, according to Newton's second law, the time domain motion equation of the platform is as follows:

$$\sum_{j=1}^{6} \left\{(M_{ij} + m_{ij}) \ddot{X}_j(t) + \int_{-\infty}^{t} \dot{X}_j(\tau) R_{ij}(t - \tau) d\tau + K_{ij} X_j(t)\right\} = F_i^{(1)}(t) \tag{14}$$

where M_{ij} is the mass matrix of the platform; m_{ij} is the added mass in the time domain, $m_{ij} = \rho \iint_{S_H} \varphi_j n_i ds$; K_{ij} is the recovery stiffness matrix; $R_{ij}(t)$ is the delay function, $R_{ij}(t)_j = \rho \iint \frac{\partial X_i(t)}{\partial t} n_i ds$; $F_i^{(-1)}(t)$ is the component of the first-order wave force on the i-th degree of freedom.

THE STRUCTURE AND WORKING PRINCIPLE OF THE PHYSICAL MODEL

ESTABLISHMENT OF PHYSICAL MODEL

In the physical model test of marine structures, a certain similarity criterion must be satisfied between the model and the prototype [18,19]. But it is not possible to satisfy all similar criteria at the same time. Therefore, according to the specific requirements and purpose of the test, the external force that plays a leading role in the test is selected to make the prototype and the model similar. This paper chooses to satisfy the geometric similarity, Strouhal similarity and Froude similarity in the model test. According to the similarity criterion, the corresponding scaling factors of relevant physical quantities in this test are shown in Table 1, where represents the prototype, represents the physical model, and represents the scaling factor.

Tab. 1. Scaling factor of physical quantities

Physical quantities	Symbol	Scaling factor	Physical quantities	Symbol	Scaling factor
Length	L_s/L_m	λ	Angle	θ_s/θ_m	1
Density	ρ_s/ρ_m	1	Frequency	f_s/f_m	$\lambda^{1/2}$
Time	t_s/t_m	$\lambda^{1/2}$	Area	A_s/A_m	λ^2
Linear velocity	v_s/v_m	$\lambda^{1/2}$	Angular velocity	ω_s/ω_m	$\lambda^{-1/2}$

Fig. 2 shows the physical model of NREL-5MW. The blade length is 0.525 m and the tower height is 0.621 m. The device is mainly composed of blades, towers, generators, batteries, hydraulic cradles, and fans, etc. In the physical model, nine eight-blade axial fans were placed side by side to simulate the effect of natural wind on the wind turbine. In order to ensure the stability of the wind speed, a fairing is installed around the fans. The working principle of the physical model device is as follows: First, select the different wind speeds required for the model experiment, which can be changed by adjusting the input power of the nine eight-blade axial fans. Then, according to the Beaufort wind scale [20], the corresponding waves at different wind speeds are selected, in which regular waves are used. Driven by the control program, the hydraulic cradle can produce heave, surge and pitch motions, which are equivalent to the motion response induced by waves acting on the floating wind turbine platform. Finally, the motion of the floating wind turbine under the coupled effect of wind and waves is simulated by the superimposed force of the fans and the hydraulic cradle.

VERIFICATION OF PHYSICAL MODEL

In order to verify the feasibility of the physical model, this paper adopts the method of comparing the results of the physical model experiment and numerical simulation. In the numerical simulation, FAST software with high fidelity results is used. Five wind speeds of 30, 35, 40, 50 and 60 m/s were selected. The comparison between the results of the physical model experiment and the numerical simulation is shown in Fig. 3.

It can be seen from Fig. 3 that the physical model experiment results are in good agreement with the numerical calculation results, except for the wind speed of 60 m/s. The variation trend of the maximum displacement of the blade tip obtained by the two is consistent.

PHYSICAL MODEL EXPERIMENT AND RESULTS ANALYSIS

In the dynamic response test of the floating wind turbine structure under the action of a typhoon, steady winds and corresponding regular waves are used according to the Beaufort wind scale. The effect of the sea current was not considered, and the propagation directions of both the wind and waves are all parallel to the y-axis, as shown in Fig. 4. In the test, the blades were set to disable rotation. According to the classification standard of typhoons, we chose 40 m/s, 50 m/s, 60 m/s (corresponding to the test wind speeds respectively of 3.65 m/s, 4.56 m/s, 5.48 m/s) as the three research target wind speeds.

(a) Tower and blades *(b) Blade* *(c) Fan* *(d) Hydraulic cradle*

Fig. 2. Schematic diagram of physical model

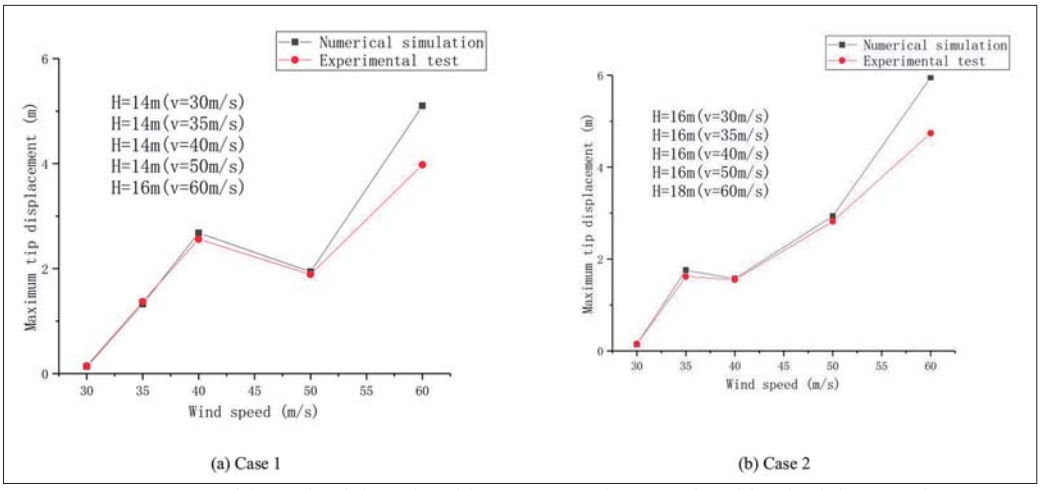

Fig. 3. Comparison of the results of physical model experiment and numerical model under different conditions

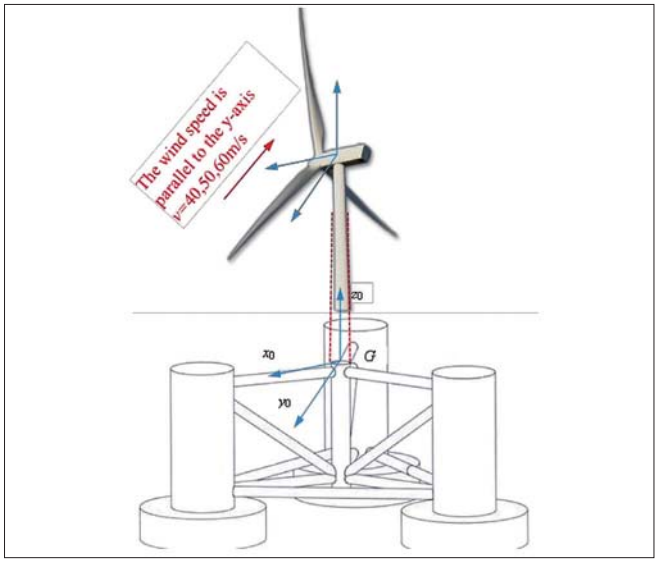

Fig. 4. Schematic diagram of the coordinate system

DYNAMIC RESPONSE ANALYSIS OF THE TOWER

Fig. 5 shows the motion response of the tower under three conditions. That is, wind speed 40 m/s, no waves; wind speed 40 m/s, wave period 25 s, wave height 16 m; and wind speed 40 m/s, wave period 26 s, wave height 16 m. Fig. 5(a) is the displacement time curve of the tower surge motion, and Fig. 5(b) is the displacement time curve of the tower sway motion.

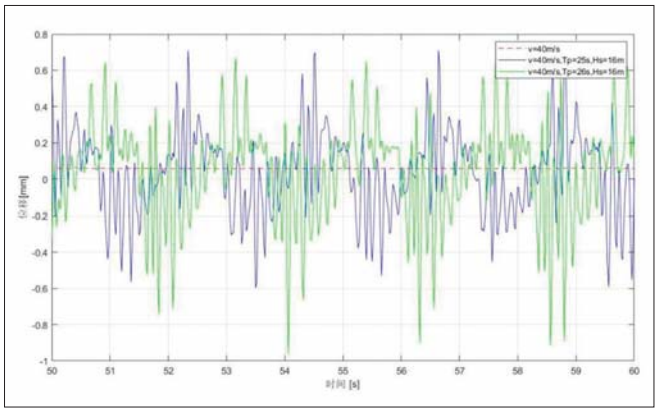

(a) Displacement time curve of the tower surge motion

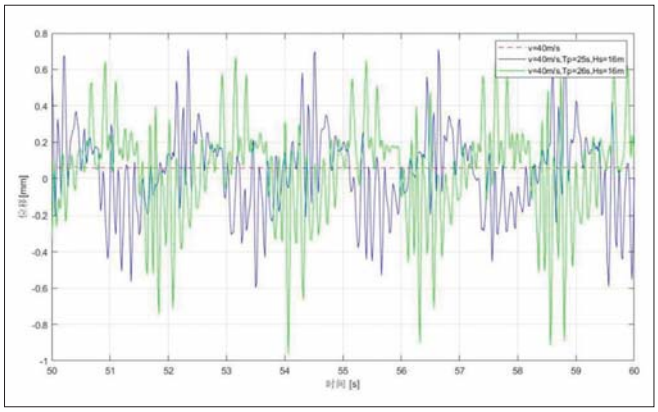

(b) Displacement time curve of the tower sway motion

Fig. 5. Displacement time curve of tower motion under 40m/s wind speed

From Fig. 5, it can be clearly seen that the tower surge or sway motion is doing a certain period of reciprocating motion. Under the action of the wind alone, the amplitude of the tower surge and sway motion is obviously smaller than under the combined effect of the wind and waves. The period of the tower surge and sway motion increases with the increase of the wave period. At the same time, the amplitude of the tower surge and sway motion also increases significantly as the wave period increases.

THE INFLUENCE OF WAVES ON TOWER MOTION

In order to study the influence of different wave heights on the tower motion, the wind speed is chosen to be 40 m/s, the wave period T_p is 27 s, and the wave heights H_S are 0 m, 14 m, 16 m and 18 m respectively. The statistical results of the dynamic response of the tower motion under the above four working conditions are shown in Table 2. The power spectral density (PSD) of the tower surge motion is obtained through fast Fourier transform (FFT), by which the displacements are transformed from the time-domain to the frequency-domain, as shown in Fig. 6.

Tab. 2. The dynamic response of the tower motion under different wave heights

Wind speed	Wave period	Wave height	Degree of freedom	Maximum value	Minimum value	Absolute value
v=40 m/s	T_p=27 s	H_s=0 m	surge (mm) sway (°)	0.07 -0.12	0.05 -0.13	0.02 0.01
		H_s=14 m	surge (mm) sway (°)	0.68 0.02	-0.88 -0.18	1.56 0.20
		H_s=16 m	surge (mm) sway (°)	0.74 0.05	-0.99 -0.22	1.73 0.27
		H_s=18 m	surge (mm) sway (°)	1.11 0.08	-1.19 -0.31	2.30 0.39

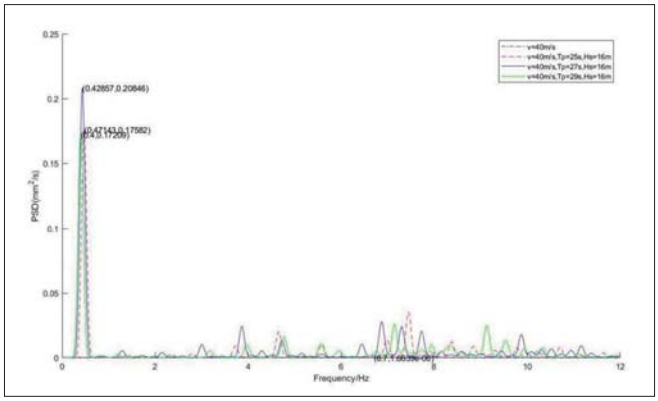

Fig. 6. PSD of the tower surge motion under different wave heights

From Table 2, it can be seen that the tower surge or sway motion is doing a certain period of reciprocating motion under different wave heights. As the wave height increases, the amplitude of both the tower surge and sway motion gradually increases. From Fig. 6, it is obvious that the PSD of the tower

Tab. 3. The dynamic response of the tower motion under different wave periods

Wind speed	Wave height	Wave period	Degree of freedom	Maximum value	Minimum value	Absolute value
v=40 m/s	H_S=16 *s*	T_P=0 *m*	surge (mm) sway (°)	0.07 -0.12	0.05 -0.13	0.02 0.01
		T_P=25 *m*	surge (mm) sway (°)	0.73 -0.01	-0.75 -0.20	1.48 0.19
		T_P=27 *m*	surge (mm) sway (°)	0.74 0.05	-0.99 -0.22	1.73 0.27
		T_P=29 *m*	surge (mm) sway (°)	0.70 -0.01	-0.72 -0.18	1.42 0.17

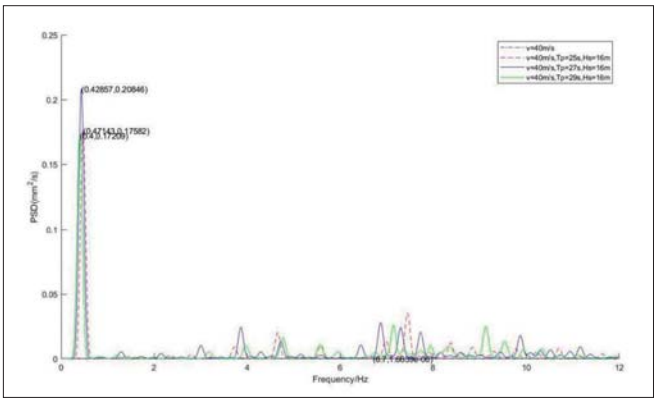

Fig. 7. PSD of the tower surge motion under different wave periods

surge motion has multiple peaks, and the frequency of the first peak of the PSD is close to that of the incident wave. In the first peak of the PSD, the peak value increases with the increase of the wave height, and the peak value in the no-wave case is significantly smaller than that in the wave case.

In order to study the influence of different wave periods on the tower motion, the wind speed v is chosen to be 40 m/s, the wave height H_S is 27 s, and the wave period T_P is 0 s, 25 s, 27 s and 29 s respectively. The statistical results of the dynamic response of the tower motion under the above four working conditions are shown in Table 3. The PSD of the tower surge motion is shown in Fig. 7.

From Table 3, it can be seen that the tower surge or sway motion is doing a certain period of reciprocating motion under different wave periods. As the wave period increases, the amplitude of both the tower surge and sway motion first increases and then decreases. From Fig. 7, it is obvious that the PSD of the tower surge motion also has multiple peaks, and the frequency of the first peak of the PSD is close to that of the incident wave. In the first peak of the PSD, the peak value first increases and then decreases with the increase of the wave period.

THE INFLUENCE OF WIND SPEED ON TOWER MOTION

In order to study the influence of different wind speeds on the tower motion, the wind speed is selected as 40 m/s, 50 m/s and 60 m/s respectively and there are no waves. The statistical results of the dynamic response of the tower motion under the above three working conditions are shown in Table 4. The PSD of the tower surge motion is shown in Fig. 8.

Tab. 4. The dynamic response of the tower motion under different wind speeds (no waves)

Wind speed	Wave condition	Degree of freedom	Maximum value	Minimum value	Absolute value
v=40 m/s	*no wave*	surge (mm) sway (°)	0.07 -0.12	0.05 -0.13	0.02 0.01
v=50 m/s		surge (mm) sway (°)	0.07 -0.10	-0.04 -0.14	0.03 0.04
v=60 m/s		surge (mm) sway (°)	0.08 -0.09	-0.02 -0.15	0.06 0.06

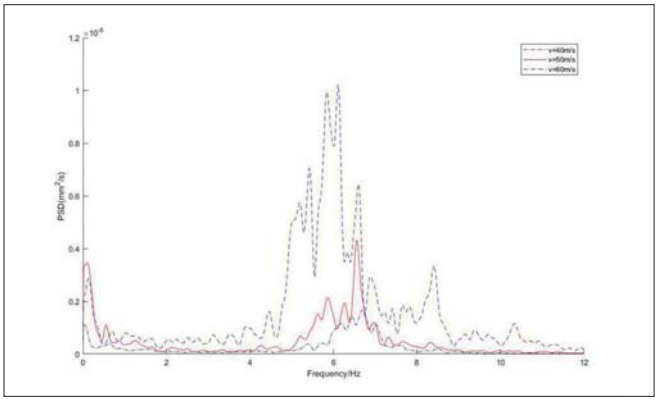

Fig. 8. PSD of the tower surge motion under different wind speeds (no waves)

From Table 4, it can be seen that in the no-wave case, the tower surge or sway motion is doing a certain period of reciprocating motion under different wind speeds. As the wind speed increases, the amplitude of both the tower surge and sway motion gradually increases. Compared with the data in Table 2 and 3, it can be seen that the influence of the wind speed on the tower motion is significantly less than that of waves. From Fig. 8, it can be seen that the PSD of the tower surge motion has multiple peaks, and the maximum peak increases with the increase of the wind speed.

Next, the influence of different wind speeds on the tower motion under the coupled action of wind and waves is studied. The wind speed is selected as 40 m/s, 50 m/s and 60 m/s respectively, the wave height H_S is 16 m, and the wave period T_P is 27 s. The statistical results of the dynamic response of the tower motion under the above three working conditions are shown in Table 5. The PSD of the tower surge motion is shown in Fig. 9.

From Table 5, it can also be seen that under the coupled effect of wind and waves, the tower surge or sway motion is doing a certain period of reciprocating motion under different wind speeds. As the wind speed increases, the amplitude of both the tower surge and sway motion gradually decreases. Compared with the data in Table 4, it can also be seen that the influence of the wind speed on the tower motion is significantly

Tab. 5. The dynamic response of the tower motion under different wind speeds (with waves)

Wave period	Wave height	Wind speed	Degree of freedom	Maximum value	Minimum value	Absolute value
T_P=27 s	H_S=16 *m*	*v*=40 *m/s*	surge (mm)	0.78	-1.3	2.10
			sway (°)	0.15	-0.23	0.48
		v=50 *m/s*	surge (mm)	0.75	-1.24	1.99
			sway (°)	0.08	-0.22	0.30
		v=60 *m/s*	surge (mm)	0.74	-0.992	1.73
			sway (°)	0.05	-0.22	0.27

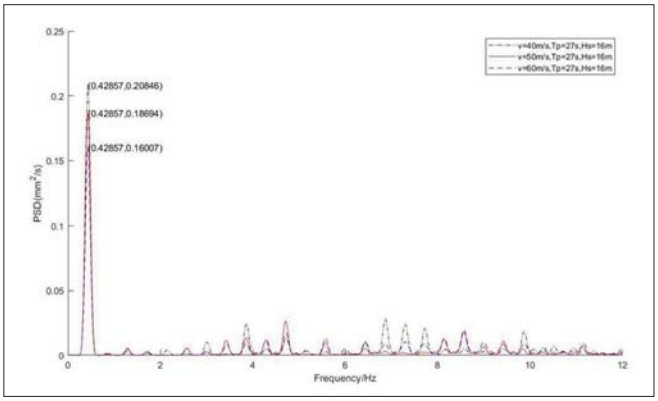

Fig. 9. PSD of the tower surge motion under different wind speeds (with waves)

less than that of waves. From Fig. 9, it can be seen that the PSD of the tower surge motion has multiple peaks, and the first peak value of the PSD decreases with the increase of the wind speed, which shows that this increase is beneficial to the survival of the platform under harsh conditions. In addition, compared with the data in Fig. 8, it can be seen that the frequency of the first peak of the PSD always appears when it is close to the incident wave frequency.

DYNAMIC RESPONSE ANALYSIS OF THE CABIN

The cabin is the most complicated part of the floating offshore wind turbine system. The power generation device, transmission system, and automatic control system are all housed in the cabin and may be damaged due to the violent motion of the cabin under the action of the wind and wave coupling. Since the propagation direction of the waves and wind is mainly along the y-direction, only the cabin acceleration in this direction is studied in the paper. The wind speed is selected as 40 m/s, 50 m/s and 60 m/s respectively, the wave height H_S is 16 m, and the wave period T_P is 27 s. The statistical results of the dynamic response of the tower motion under the above three working conditions are shown in Table 6. The PSD of the tower surge motion is shown in Fig. 10.

From Table 6, it can be seen that the cabin acceleration is also doing a certain reciprocating motion under the coupled effect of wind and waves. As the wind speed increases, the amplitude of the cabin acceleration gradually decreases, which shows that the intensity of the cabin motion is alleviated as

Tab. 6. Cabin acceleration in the y-direction

Wave period	Wave height	Wind speed	Maximum value (m^2/s)	Minimum value (m^2/s)	Absolute value (m^2/s)
T_P=27 s	H_S=16 *m*	*v*=40 *m/s*	4.73	-7.30	12.03
			4.68	-6.08	10.76
			4.59	-5.89	1.48

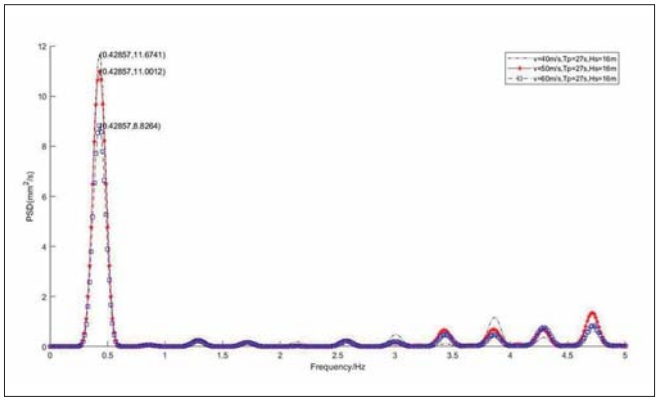

Fig. 10. PSD of the cabin acceleration

the wind speed increases. From Fig. 10, it can be seen that the PSD of the cabin acceleration has multiple peaks, and the maximum peak decreases with the increase of the wind speed. The maximum peak appears when it is close to the incident wave frequency.

CONCLUSION

This paper takes the NREL-5MW floating offshore wind turbine as the research object, and its basic structure and working principle are introduced. In order to study the dynamic response of floating offshore wind structures under typhoons, the influence of the wave and wind speed on the dynamic response of the tower and cabin is studied. According to the structural characteristics and working principle of the NREL-5MW wind turbine, a physical model with a scale ratio of 1:120 was established. The physical model uses fans and hydraulic cradles to simulate the effects of wind and waves on the platform in the ocean. The reliability of the physical model is verified by comparing the results of the physical model test and the numerical simulation. Based on the above physical model experiment results, the following conclusions can be drawn:

(1) Under the coupled effect of wind and waves, the tower surge or sway motion is doing a certain period of reciprocating motion. The influence of the wind speed on the tower surge or sway motion is significantly less than that of waves.
(2) Under the coupled effect of wind and waves, the amplitude of both the tower surge and sway motion gradually increases with the increase of the wave height. The PSD of the tower surge motion has multiple peaks, and the frequency of the first peak of the PSD is close to that of the incident wave. In the first peak of the PSD, the peak value increases with

the increase of the wave height, and the peak value in the no-wave case is significantly smaller than that in the wave case.

(3) Under the coupled effect of wind and waves, the amplitude of both the tower surge and sway motion first increases and then decreases with the increase of the wave period. In the first peak of the PSD of the tower surge motion, the peak value first increases and then decreases with the increase of the wave period.

(4) In the no-wave case, the tower surge or sway motion is doing a certain period of reciprocating motion under different wind speeds. As the wind speed increases, the amplitude of both the tower surge and sway motion gradually increases. In the PSD of the tower surge motion, the maximum peak increases with the increase of the wind speed.

(5) Under the coupled effect of wind and waves, the tower surge or sway motion is doing a certain period of reciprocating motion under different wind speeds. As the wind speed increases, the amplitude of both the tower surge and sway motion gradually decreases. In the PSD of the tower surge motion, the first peak value decreases with the increase of the wind speed, which shows that this increase is beneficial to the survival of the platform under typhoons. And the frequency of the first peak of the PSD always appears when it is close to the incident wave frequency.

(6) The cabin acceleration is also doing a certain reciprocating motion under the coupled effect of wind and waves. As the wind speed increases, the amplitude of the cabin acceleration gradually decreases. The cabin acceleration has multiple peaks, and the maximum peak decreases with the increase of the wind speed. The maximum peak appears when it is close to the incident wave frequency.

The above conclusions can provide a certain reference value for the design of floating offshore wind turbines in the deep sea.

ACKNOWLEDGEMENTS

This research was supported by the National Natural Science Foundation of China (51679217), "Pioneer" and "Leading Goose" R&D Program of Zhejiang (2022C03023).

REFERENCES

1. D. Gielen, F. Boshell, D. Saygin, et al. 'The role of renewable energy in the global energy transformation', Energy Strategy Reviews. 2019, doi: 10.1016/j.esr.2019.01.006

2. P. Veers, K Dykes, E. Lantz, et al. 'Grand challenges in the science of wind energy', Science. 2019, doi: 10.1126/science.aau2027

3. K. Y. Oh, W. Nam, M. S. Ryu, et al. 'A review of foundations of offshore wind energy convertors: Current status and future perspectives', Renewable and Sustainable Energy Reviews. 2018, doi: 10.1016/j.rser.2018.02.005

4. Y. Li, X. Huang, K. F. Tee, et al. 'Comparative study of onshore and offshore wind characteristics and wind energy potentials: A case study for southeast coastal region of China', Sustainable Energy Technologies and Assessments. 2020, doi: 10.1016/j.seta.2020.100711

5. Z. Ren, A. S. Verma, Y. Li, et al. 'Offshore wind turbine operations and maintenance: A state-of-the-art review', Renewable and Sustainable Energy Reviews. 2021, doi: 10.1016/j.rser.2021. 110886

6. A. Tomporowski, I. Piasecka, J. Flizikowski, et al. 'Comparison analysis of blade life cycles of land-based and offshore wind power plants', Polish Maritime Research. 2018, doi: 10.2478/pomr-2018-0046

7. Y. Zhou, Q. Xiao, Y. Liu, et al. 'Numerical modelling of dynamic responses of a floating offshore wind turbine subject to focused waves', Energies. 2019, doi: 10.3390/en12183482

8. [8] L. Chen, B. Basu. 'Wave-current interaction effects on structural responses of floating offshore wind turbines', Wind Energy. 2019, doi: 10.1002/we.2288

9. D. Tang, M. Xu, J. Mao, et al. 'Unsteady performances of a parked large-scale wind turbine in the typhoon activity zones', Renewable Energy. 2020, doi: 10.1016/j.renene.2019.12.042

10. R. Han, L. Wang, T. Wang, et al. 'Study of Dynamic Response Characteristics of the Wind Turbine Based on Measured Power Spectrum in the Eyewall Region of Typhoons', Applied Sciences. 2019, doi: 10.3390/app9122392

11. N. Aggarwal, R. Manikandan, N. Saha. 'Nonlinear short term extreme response of spar type floating offshore wind turbines', Ocean Engineering. 2017, doi: 10.1016/j.oceaneng.2016.11.062.

12. T. T. Tran, D. H. Kim. 'The platform pitching motion of floating offshore wind turbine: A preliminary unsteady aerodynamic analysis', Journal of Wind Engineering and Industrial Aerodynamics. 2015, doi: 10.1016/j.jweia.2015.03.009

13. D. Roddier, C. Cermelli, A. Aubault, et al. 'WindFloat: A floating foundation for offshore wind turbines', Journal of Renewable and Sustainable Energy. 2010, doi: 10.1063/1.3435339

14. Z. Chen, X. Wang, Y. Guo, et al. 'Numerical analysis of unsteady aerodynamic performance of floating offshore wind turbine under platform surge and pitch motions', Renewable Energy. 2021, doi: 10.1016/j.renene.2020.10.096

15. T. Ishihara, Y. Liu. 'Dynamic Response Analysis of a Semi-Submersible Floating Wind Turbine in Combined Wave

and Current Conditions Using Advanced Hydrodynamic Models', Energies. 2020, doi: 10.3390/en13215820

16. G. Clauss, E. Lehmann, C. Östergaard. Offshore Structures: volume I: 'Conceptual design and hydromechanics'. Springer, 2014.

17. W. W. Massie, J. M. Journée. 'Offshore hydromechanics'. Delft University of Technology: Delft, The Netherlands, 2001.

18. Y. Fang, et al. 'Numerical analysis of aerodynamic performance of a floating offshore wind turbine under pitch motion', Energy. 2020, doi:10.1016/j.energy.2019.116621

19. S. K. Chakrabarti. Offshore structure modeling'. Vol. 9. World Scientific, 1994.

20. L. Yu, C. Ying. 'CFD analysis for a set of axial fan array to produce inflow for wind turbine model test', 29th International Ocean and Polar Engineering Conference. OnePetro, 2019.

CONTACT WITH THE AUTHORS

Junlai Li
e-mail: 11059979@qq.com

Weiguo Wu
e-mail: mailjt@163.com

Wuhan University of Technology
No.1178, Heping Avenue
430063 Wuhan, Hubei
China

Yu Wei
e-mail: 117597614@qq.com

Yu Shu
e-mail: 415672729@qq.com

Zhiqiang Lu
e-mail: 1065861814@qq.com

Wenbin Lai
e-mail: 630880804@qq.com

Panpan Jia
e-mail: 296167636@qq.com

Cheng Zhao
e-mail: s19082400004@zjou.edu.cn

Yonghe Xie
e-mail: xieyh@zjou.edu.cn

ZheJiang Ocean University
No.1, Haida South Road
Lincheng Changzhi Island
316022 Zhoushan, Zhejiang
China